Seidel optical aberrations and optimum truncated Gaussian beams on intersatellite free-space optical communications

Badas Aldecocea, M.; Piron, P.; Bouwmeester, J.; Saathof, R.; Loicq, Jérôme

DOI
10.1364/OE.565652

Publication date
2025

Document Version
Final published version

Published in
Optics Express

Citation (APA)
Badas Aldecocea, M., Piron, P., Bouwmeester, J., Saathof, R., & Loicq, J. (2025). Seidel optical aberrations and optimum truncated Gaussian beams on intersatellite free-space optical communications. *Optics Express*, *33*(16), 33686-33703. Article 33686. https://doi.org/10.1364/OE.565652

Research Article | Vol. 33, No. 16 / 11 Aug 2025 / Optics Express 33686
Optics EXPRESS

Seidel optical aberrations and optimum truncated Gaussian beams on intersatellite free-space optical communications

MARIO BADÁS,[1,*] PIERRE PIRON,[1] JASPER BOUWMEESTER,[1] RUDOLF SAATHOF,[1] AND JÉRÔME LOICQ[1,2]

[1]Department of Space Engineering, Delft University of Technology, Kluyverweg 1, 2629 HS Delft, Netherlands
[2]University of Liège, STAR Institute, Avenue du Pré Aily, 4031 Liège, Belgium
[*]m.badasaldecocea@tudelft.nl

Abstract: Intersatellite free-space optical communications are the backbone of the future high-speed global communication networks. In orbit, thermo-mechanical loads create perturbations that detriment the performance of these links. Among these perturbations, the transmitter pointing jitter and optical aberrations are of special relevance. We present an analysis of the coupled effects of transmitter pointing jitter and optical aberrations on intersatellite free space optical communications. A mathematical model is presented to evaluate the performance of average bit error probability, probability of outage, and reliability on intersatellite free space optical communication links subjected to these perturbations. Furthermore, the optimum non-aberrated truncated Gaussian beams are obtained for each of these performance parameters for different telescope architectures. The results demonstrate that the performance parameters are highly sensitive to the optimal far-field irradiances. These optimum operation points are then perturbed by Seidel aberrations to study the effect of these aberrations in the system. The results show that optical communication terminals are most sensitive to coma aberrations, mainly due to the induced apparent angle of arrival on the beacon beam. Finally, Monte Carlo simulations of combinations of Seidel aberrations show a strong dependency on the telescope architecture of the sensitivity of the communication performance parameter to the magnitude of the optical aberrations.

1. Introduction

The increasing demand of more secure and higher data throughput in global communication networks, locates free space optical communication (FSOC) as a strong alternative to the current radio-frequency-based systems. The high directionality of laser beams used in FSOC can be exploited for both security and power savings purposes. In constructing a global FSOC network, intersatellite optical links are key for bridging large distances through space. In addition, the satellite optical terminals in space are also crucial for the future space-based quantum communication systems [1].

Optical terminals in space are subjected to the harsh and rapidly changing space environment. In orbit thermo-mechanical loads will create microvibrations and deformations that deviate the system from its ideal operation. These microvibrations will materialize into pointing jitter deviations of the transmitted laser beam, stochastically deviating its optical axis from the receiver. Although this effect is mitigated with coarse and fine pointing systems, there will always remain a residual pointing jitter that will detriment the performance of the system. These pointing jitter, among with the finiteness of the transmitter aperture, will limit the exploitation of the high

#565652 https://doi.org/10.1364/OE.565652
Journal © 2025 Received 21 Apr 2025; revised 5 Jul 2025; accepted 20 Jul 2025; published 31 Jul 2025

Optics EXPRESS

directionality of the transmitted laser beam. Along with this pointing jitter, the thermo-mechanical loads will also create optical aberrations on the terminals, which will in turn affect the system's performance (see Fig. 1). These aberrations will affect both the transmitted communication beam and the received beacon beam, changing their respective irradiances and therefore altering the performance of the system. When acting as a receiver, the satellite optical terminal will be subjected to the same loads too. This will create a stochastic incoming angle of arrival and reduced coupling performance (see Fig. 1). However, the latter effects will not be covered in this study as they are the focus of other studies [2–5]. In general, the effect of pointing jitter and optical aberrations is that of reducing the performance of intersatellite optical communications, e.g. data loss on LEO-GEO links.

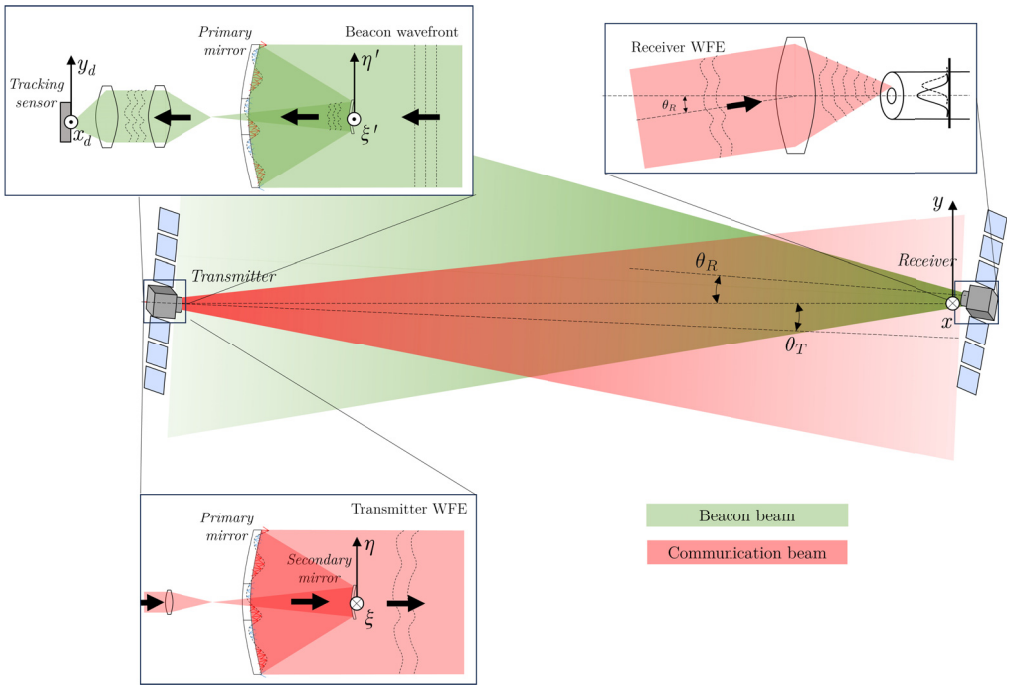

Fig. 1. Illustration of the effect of the transmitter and receiver wavefront errors and pointing jitters. θ_T and θ_R represent the transmitter pointing error and receiver angle of arrival at a certain instant of time, respectively. In the top left figure, only the sensor of the tracking system is shown for simplicity, while the complete tracking system would also have actuators (i.e. coarse and fine-pointing assemblies).

Analyzing the effect of the coupled phenomena given by the transmitter pointing jitter and optical aberrations is necessary for establishing requirements for the optical design of space terminals. On the one side, there is a fair amount of literature analyzing the effect of pointing jitter on intersatellite optical links, such as the early works by Kiasaleh and Toyoshima to mention a few [6,7]. Analyses combining the effect of the pointing jitter and other in orbit perturbations are can be found in Refs. [8,9]. Furthermore, the effect of transmitter optical aberrations on the mutual alignment error has also been studied in depth [10–14]. The effect of optical aberrations in the propagation of a Gaussian beam can also be found in the literature [15–19]. Finally, a simplified analysis of the combined effect of transmitter pointing jitter and optical aberrations has been developed by Yang et al. [20,21]. However, the combined effect of transmitter pointing jitter and optical aberrations, considering the mutual alignment error (or the related apparent angle of arrival that is defined later in the present work) and the finite aperture effects, on

Optics EXPRESS

different communication parameters, is lacking in the literature. In this work, we present a model that encompasses all this coupled phenomena, enabling a more accurate evaluation of the perturbations mentioned. Our work will provide insight in the interplay between these perturbations and how the communication performance of the system is affected (Section 3.2). Furthermore, it will help determine the requirements for admissible pointing jitter and optical aberrations in FSOC satellite terminals. In summary, this work aims to provide a step forward in developing the next generation of reliable intersatellite optical communications.

We first explain the mathematical model developed to evaluate the impact of pointing jitter and transmitter optical aberrations in Section 2. The effects of optical aberrations on both the transmitted communication beam and the received beacon beam are accounted for through wave optics propagation as presented in Sections 2.1 and 2.2. The mathematical models to compute the received power statistics due to the stochastic transmitter pointing jitter are presented in Sections 2.3 and 2.4. From these statistics, different communication performance parameters can be obtained (Section 2.5). Using the proposed model, the optimum far-field irradiance distributions for different communication performance parameters, when considering a truncated Gaussian beam are obtained for different transmitter architectures (Section 3.1). This is done considering only the transmitter pointing jitter, without optical aberrations. These optimized solutions are then perturbed with transmitter optical aberrations to evaluate the impact of these on the communication performance. An analysis is presented showing the effect of each of the Seidel aberrations for different telescope architectures. Finally, the combined effect of these Seidel aberrations acting altogether is assessed statistically through Monte Carlo simulations.

2. Wave optics propagation and communication performance

In this section, the mathematical model to compute the performance of an intersatellite link under transmitter pointing jitter and wavefront errors is presented. Firstly, the computational optical model to obtain the far-field diffraction pattern is presented. Secondly, the effect of the optical aberrations on the received beacon, which materialize as mutual alignment errors, are presented. Then, the far-field irradiance and the pointing jitter statistics are combined to obtain the statistics of the received power. Finally, the received power statistics are used to compute different communication performance parameters of the intersatellite link. The block diagram in Fig. 2 shows the overview of the steps followed in the model.

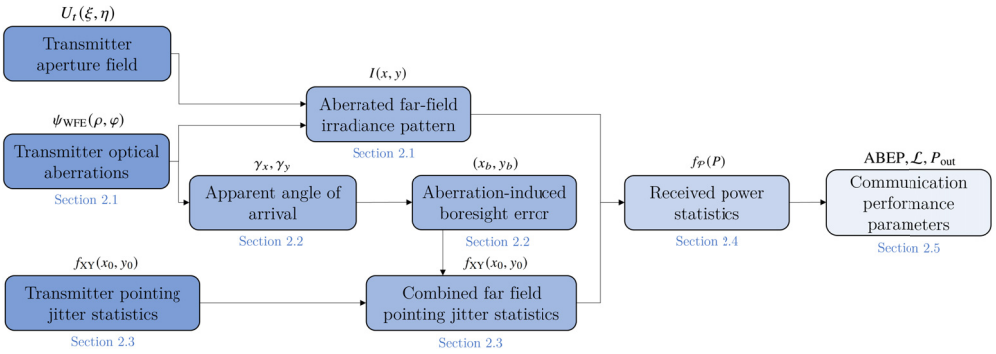

Fig. 2. Diagram of the steps of the mathematical model to compute the effect of optical aberrations on intersatellite FSOC. The mathematical expression and the relations between them are presented in the respective sections of the paper.

Optics EXPRESS

2.1. Wave optics propagation: far-field diffraction patterns

For a complex electromagnetic scalar field in the transmitter aperture plane (including the optical aberrations under study), the far-field irradiance pattern at the receiver aperture plane can be obtained through Fourier optics. A Gaussian beam is considered as the output of the laser source in the transmitter [7]. However, due to the diffraction effects of the transmitter aperture and the optical aberrations, the outgoing beam is no longer purely Gaussian. Given that different transmitter telescope architectures, will yield different far-field diffraction patterns, three different architectures are considered in this work. In Fig. 3 these architectures are illustrated. Figure 3(a) shows the case of a telescope-centered Gaussian beam with a central *obscuration* due to the secondary mirror. Figure 3(b) shows the case for a *clear* aperture telescope. This case is also representative of a clear refractive telescope, not necessarily an off-axis reflective one as shown in the figure. Figure 3(c) shows the case in which the central obscuration of the telescope is avoided by using an off-axis *subaperture*. In Section 3.2 the differences between the clear and subaperture architectures are emphasized. In the nominal case (without optical aberrations), the design of the system has to be done so that the outgoing beam contains as much of the power available, and the far-field irradiance of the beam is optimum for the given pointing jitter [7]. The electrical field for a Gaussian beam of wavelength λ in a homogeneous medium with index of refraction n is

$$U_G(x,y,z) = U_0 \frac{w_0}{w(z)} \exp\left(-\frac{x^2+y^2}{w(z)^2}\right) \exp\left[-i\left(kz + k\frac{x^2+y^2}{2R(z)} - \nu(z)\right)\right] \tag{1}$$

where

$$w(z) = w_0\sqrt{1+\left(\frac{z}{z_R}\right)^2} \qquad R(z) = z\left[1+\left(\frac{z_R}{z}\right)^2\right] \qquad \nu(z) = \arctan\left(\frac{z}{z_R}\right)$$

$w(z)$ is the beamwidth of the beam at a distance z from the beamwaist, $R(z)$ is the radius of curvature of the Gaussian beam wavefront, $\nu(z)$ is the Gouy phase and $z_R = \pi w_0^2 n/\lambda$ is the Rayleigh distance. When transmitting a Gaussian beam, the finiteness of the telescope aperture will truncate and obscure the Gaussian beam to a higher or lower extent. The need for each of these different architectures is given by the telescope design trade-off [22]. For each of these architectures, the divergence of the outgoing beam can be adjusted by adjusting the beamwidth $w(z)$ and the curvature of the wavefront $R(z)$ in the transmitter's aperture plane. Instead, in this paper, the outgoing Gaussian beam will be characterized by the beamwidth $w(z) = w_z$ at the transmitter aperture plane, and the underlying beamwaist w_0 (see Fig. 3(c)). In the Supplement 1, a simplified explanation of how these parameters can be adjusted through optical design of the system is presented by using the ABCD matrix method.

Depending on the transmitter telescope architecture considered, the field in the transmitter aperture is given by

$$U_t(\xi,\eta) = U_G(\xi,\eta,z_t)\ \mathcal{A}(\xi,\eta)\ \exp\left[j\,\psi_{\mathrm{WFE}}(\xi,\eta)\right] \qquad \text{Fig. 3a and 3b} \tag{2}$$

$$U_t(\xi,\eta) = U_G(\xi,\eta-\eta_0,z_t)\ \mathcal{A}(\xi,\eta)\ \exp\left[j\,\psi_{\mathrm{WFE}}(\xi,\eta)\right] \qquad \text{Fig. 3c} \tag{3}$$

where η_0 corresponds to the decentering of the beam axis with respect to the telescope optical axis and $z_t = z_R\sqrt{(w_z/w_0)^2-1}$ is given by the beamwidth at the transmitter aperture w_z and the underlying beamwaist w_0. The optical aberrations have been included via the additional phase

Optics EXPRESS

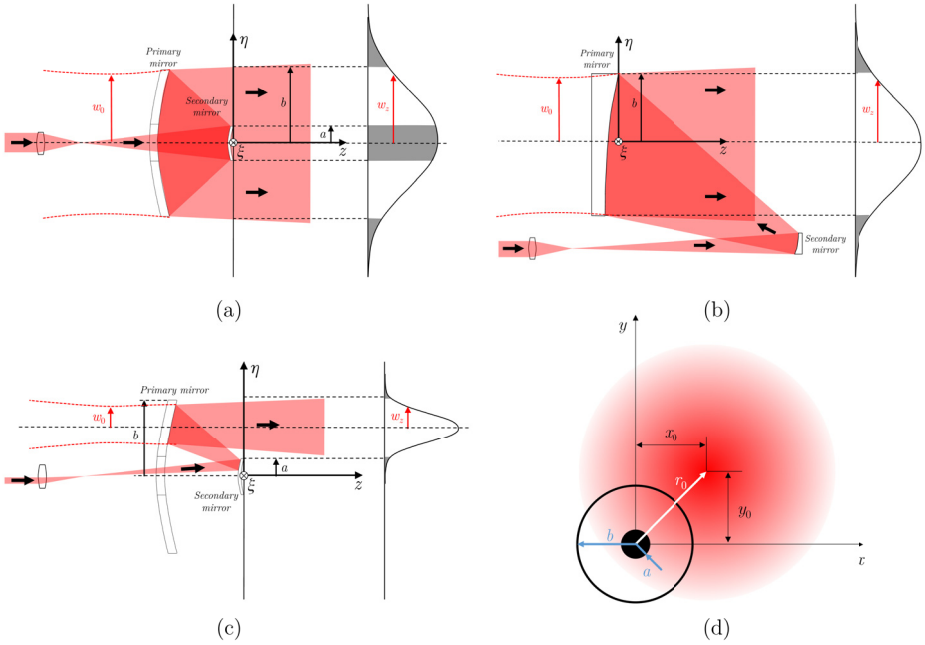

Fig. 3. (a)-(c) Transmitted beam truncation and obscuration for three different transmitter architectures analyzed: (a) obscured, (b) clear, and (c) subaperture architectures. (d) The receiver's aperture plane shows the far-field irradiance pattern at a certain instant with pointing error (x_0, y_0) as seen from the inside of the receiver.

$\psi_{\text{WFE}}(\xi,\eta)$, and $\mathcal{A}(\xi,\eta)$ is the transmitter aperture function is given by

$$\mathcal{A}(\xi,\eta) = \begin{cases} 1 & \text{if} \quad a \le \sqrt{\xi^2+\eta^2} \le b \\ 0 & \text{else} \end{cases} \tag{4}$$

where b and a are the primary and secondary mirror radii, respectively. The clear aperture architecture in Fig. 3(b), has no secondary mirror, i.e. $a = 0$. In this model, the effects of the transmitter's optical aberrations are considered as if they were being applied in the aperture plane of the transmitter. This is because most of the optical aberrations due to in-orbit thermo-mechanical loads, will happen in the primary mirror of the transmitter's telescope. This is usually the optical component that is the largest and most exposed to the space environmental loads [10]. The additional phase $\psi_{\text{WFE}}(\xi,\eta)$ representing the optical aberrations can be expressed in polar coordinates using the Zernike polynomials $Z_n^m(\rho,\varphi)$ [23]

$$\psi_{\text{WFE}}(\rho,\varphi) = \sum_{n=0}^{\infty}\left(\sum_{m=-n}^{n} a_{nm}\, Z_n^m(\rho,\varphi)\right) \tag{5}$$

where a_{nm} are the coefficients corresponding to the radial index n and the azimuthal index m. Figure 4 shows the first Zernike polynomials along with their classical denominations. To compute the far-field irradiance distribution, the Fresnel equation for wave propagation can be numerically evaluated with [24]

$$U_r(x,y) = \frac{e^{jk\Delta z}}{j\lambda\Delta z}\, e^{j\frac{k}{2\Delta z}(x^2+y^2)} \iint_{\mathbb{R}^2} \left\{U_t(\xi,\eta)\, e^{j\frac{k}{2\Delta z}(\xi^2+\eta^2)}\right\} e^{-j\frac{2\pi}{\lambda\Delta z}(x\xi+y\eta)} d\xi d\eta \tag{6}$$

Optics EXPRESS

where $U_r(x, y)$ is the field in the receiver aperture plane at a given distance Δz from the transmitter, and $U_t(\xi, \eta)$ is the field in the transmitter aperture plane. In reality, the receiver plane is tilted a small angle with respect to the perpendicular plane to the transmitter optical axis (see Fig. 1). This tip-tilt is the combination of both the transmitter and receiver angular pointing jitters. This deviation would create not only a displacement as seen by the receiver considered in Section 2.3, but also a tip-tilt of the received field [25–28]. However, for the small angular pointing jitters involved in satellite optical communications, this effect is negligible. Combining the equations above, Eq. (6) can be numerically evaluated using the Fast Fourier Transform to obtain the far-field $U_r(x, y)$ on the receiver aperture plane. Finally, the far-field irradiance distribution in the receiver's aperture plane is obtained by simply evaluating $I_r(x, y) = |U_r(x, y)|^2/2\varsigma_0$ where the wave impedance is $\varsigma_0 = 377\ \Omega$ for free space. The source of the optical aberrations will be in orbit variations of temperature [10], hence the variation of the far-field irradiance shape will occur on the order of minutes at least [29]. Therefore, the effect of the optical aberrations is considered quasi-static compared to the pointing jitter dynamics, the later having a characteristic time on the order of milliseconds [30,31].

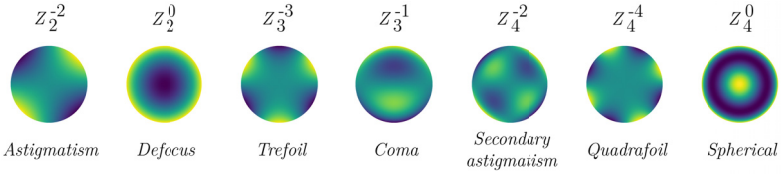

Fig. 4. Zernike polynomials $Z_n^m(\rho, \varphi)$ for different radial and azimuthal indices, n and m respectively

2.2. Apparent angle of arrival and mutual alignment error

In the previous section, the model to compute the effect of the transmitter optical aberrations in the far-field irradiance pattern has been presented. Furthermore, these aberrations will also affect the diffraction pattern on the tracking detector plane of the beacon coming from the receiver (see Fig. 1). As a result of the aberrated beacon image on the tracking sensor, an *apparent* angle of arrival of the beacon signal will be detected. This artifact, created by the optical aberrations, will command the tracking system to point the outgoing beam towards the direction of this apparent angle of arrival. In this paper, we consider that the tracking sensor uses a center of gravity algorithm to detect the direction of the incoming beacon. The type of algorithm that can be used depends on the type of tracking sensor considered. When using a quadrant photodiode with an axially symmetric irradiance shape, the usual quadrant algorithm can yield similar results to that of the center of gravity algorithm [32]. When using a higher spatial resolution tracking sensor (e.g. a CCD), the center of gravity and maximum irradiance algorithms are mostly used. For a comparison of the apparent angle of arrival obtained when using a center of gravity or maximum irradiance algorithms, see the Supplement 1.

At the large distances involved in intersatellite optical communications and the big divergence used for the beacon beam, the beacon field is seen as a uniform plane wave in the transmitter aperture plane. When the transmitter is pointing directly in the line of sight of the incoming beacon, the beacon's complex field in the transmitter aperture plane (considering unit amplitude of the field) is given by

$$U_b(\xi', \eta') = \mathcal{A}(-\xi', \eta')\ \exp\left[-j\,\psi_{\mathrm{WFE}}(-\xi', \eta')\right] \tag{7}$$

where again the optical aberrations and aperture diffraction effects have been included. The negative sign in the phase field of the optical aberrations represents the fact that the received

Optics EXPRESS

beacon sees the inverse aberration of what the transmitted beam sees (see Fig. 1). Furthermore, the (ξ', η') reference system used, is consistent for propagating the received beacon towards the transmitter terminal instead of outwards (see Supplement 1 for more details on the reference systems used). The complex field in the tracking sensor plane, U_d, is obtained via Fraunhofer diffraction equation [24], with an effective focal length f that focuses the incoming beacon to the tracking sensor plane,

$$U_d(x_d, y_d) = \frac{1}{j\lambda f}\, e^{j\frac{k}{2f}(x_d^2+y_d^2)} \iint_{\mathbb{R}^2} U_b(\xi', \eta')\, e^{-j\frac{2\pi}{\lambda f}(x_d\xi'+y_d\eta')} d\xi' d\eta' \tag{8}$$

The irradiance can then be computed as $I_d = |U_d(x_d, y_d)|^2/2\varsigma_0$. Finally, by computing the center of gravity (x_G, y_G) of this irradiance field as

$$x_G = \frac{\iint I_d(x_d, y_d) \cdot x_d \; dx_d dy_d}{\iint I_d(x_d, y_d)\; dx_d dy_d} \qquad y_G = \frac{\iint I_d(x_d, y_d) \cdot y_d \; dx_d dy_d}{\iint I_d(x_d, y_d)\; dx_d dy_d} \tag{9}$$

the apparent angle of arrival directions on the tracking detector reference system can be obtained as

$$\gamma_{d,x} = \frac{x_G}{f} \qquad \gamma_{d,y} = \frac{y_G}{f} \tag{10}$$

As the tracking algorithm corrects for this apparent angle of arrival, the transmitted beam will be mispointed from the real beacon direction (real direction of the receiver terminal) by a static boresight error. Hence, the transmitted beam will be pointing in the direction given by the directional angles $(\gamma_x, \gamma_y) = (\gamma_{d,x}, -\gamma_{d,y})$ as seen by the transmitter's outgoing reference system (see the Supplement 1 for more details on the reference systems used). Toyoshima et al. [10] define the mutual alignment error as the angle between the direction of the apparent angle of arrival and the direction of the maximum irradiance of the aberrated transmitted beam. While the apparent angle of arrival tells us the direction error between the real receiver direction and the optical axis of the transmitted beam, the mutual alignment error accounts for the direction error between the real receiver direction and the peak irradiance direction of the transmitted beam. As commented in the previous section, the variation of the optical aberrations is considered to be quasi-static compared to the dynamics of the pointing jitter (which occur at ~kHz, see Ref. [29]). Therefore, the apparent angle of arrival will be treated statically, including an additional boresight error in the transmitter pointing jitter statistics.

2.3. Transmitter pointing jitter

Along with the effects of the transmitter optical aberrations presented in the previous sections, in-orbit microvibrations will generate a pointing jitter of the transmitted beam's optical axis. Although this is usually mitigated by the pointing system, there will always remain a residual pointing jitter affecting the transmitted beam [29]. This jitter will create a stochastic fading of the received power that will affect the performance of the system as presented in the next section. The transmitter angular pointing jitter is usually characterized by a centered bivariate Gaussian distribution [7,33,34]. Theoretically, this assumption is justified by the central limit theorem given that the transmitted pointing jitter statistics are determined by a large number of variables [35]. Furthermore, experimental verification of the previous can be found in the literature [30,31,36,37]. For the small angle approximation, it can be shown that this translates into a decenter error between the transmitted beam center and the receiver's axis (see Fig. 3(d)), characterized by a centered bivariate Gaussian distribution. Finally, considering that the standard deviation in x and y axes are the same (or in azimuth and elevation angles in the transmitter

Optics EXPRESS

pointing), the probability density function (PDF) of the pointing jitter is given by

$$f_{\mathrm{XY}}(x_0, y_0) = \frac{1}{2\sigma^2} \exp\left[-\frac{(x_0 - x_b)^2 + (y_0 - y_b)^2}{2\sigma^2}\right] \tag{11}$$

where (x_0, y_0) are the coordinates of the instantaneous error, (x_b, y_b) are the coordinates of the boresight error and σ is the standard deviation of the bivariate Gaussian distribution. Under the small angle approximation, the angular pointing jitter is defined as $\sigma_\theta = \sigma/\Delta z$, where Δz is the link distance. In our model, the only source of boresight error is the apparent angle of arrival explained in Sec. 2.2. For zero boresight error, the previous PDF is converted to a Rayleigh distribution, $f_{\mathcal{R}}(r)$, in radial coordinates. When the problem in hands is fully axially symmetric, this distribution can be useful [38].

2.4. Received power statistics

As seen by the receiver aperture plane, the effect of the thermo-mechanically induced optical aberrations presented above is to have an aberrated far-field irradiance pattern (Section 2.1), that is quasi-statically displaced by the mutual alignment error (Section 2.2). Furthermore, the transmitter's angular pointing jitter stochastically further deviates the center of the aberrated far-field from the receiver aperture plane (Section 2.3). All these effects together create a fluctuation of the power collected by the receiver aperture. In this section, the expressions to obtain the received power statistics from the far-field irradiance pattern and the pointing jitter statistics are presented.

The location of the far-field irradiance distribution in the receiver's aperture plane is affected by the transmitter pointing jitter. This stochastic process will produce received power dynamics, that will degrade the performance of the system. The received power as a function of the location of the center of the transmitted beam, given by the coordinates (x_0, y_0), can be computed through a bidimensional convolution of the receiver's aperture pupil and the far-field irradiance at the receiver's aperture plane (see Fig. 3(d))

$$P = g(x_0, y_0) = \iint_{\mathbb{R}^2} I(x, y)\, \mathcal{A}(x - x_0, y - y_0)\, dxdy = \mathcal{F}^{-1}\{\mathcal{F}(I) \cdot \mathcal{F}(\mathcal{A})\} \tag{12}$$

where $\mathcal{A}(x, y)$ is the pupil function of the receiver and the convolution theorem has been applied to obtain the last equality in terms of Fourier transforms. This work considers symmetric intersatellite links, in which the pupil function of the receiver is the same as the transmitter's (see Eq. (4)). When the change on the far-field irradiance across a length equal to the diameter of the receiver telescope is negligible, the previous expression can be simplified as $g(x_0, y_0) \approx A \cdot I(x_0, y_0)$, where A is the total area of the receiver's aperture.

To evaluate the performance of a communication system, the received power statistics are needed. Considering a slow fading channel, in which the modulation frequency of the communication signal is orders of magnitude higher than the dynamics of the power fading, the received power can be characterized by a PDF to later obtain communication performance parameters [39]. As the dynamics of the pointing jitter are on the order of kHz, compared to the usual MHz modulation frequencies, the slow fading channel is a good approximation for our work [29]. To obtain the PDF of the received power, the power as a function of the displacement of the beam (Eq. (12)) can be combined with the PDF of the position of the center of the beam in the receiver aperture plane (Eq. (11)). Using these functions and the expression to obtain PDFs from statistically dependent variables [40], the PDF of the received power can be obtained as

$$f_{\mathcal{P}}(P) = \iint_{-\infty}^{\infty} f_{\mathrm{XY}}(x_0, y_0)\, \delta\left[P - g(x_0, y_0)\right]\, dx_0\, dy_0 \tag{13}$$

where $\delta(x)$ is the Dirac delta function. When both the irradiance field and the transmitter pointing jitter PDF are axially symmetric the simplified equations presented in Ref. [38] can be used.

Optics EXPRESS

However, in general, the truncation geometry, the optical aberrations and the mutual alignment error will break this axial symmetry and therefore, the expressions above are required to obtain the received power statistics. By normalizing the received power P by the average transmitted power P_t, the PDF of the channel loss $f_{\mathcal{P}}(h)$ can be obtained, where $h = P/P_t$.

2.5. Communication performance parameters

In this section, we present the parameters that characterize the performance of an intersatellite optical communication system. For a more detailed discussion on these and other communication performance parameters, see the Supplement 1. We will be considering three main performance parameters in this work: Average Bit Error Probability (ABEP), probability of outage (P_{out}), and the reliability ($\mathcal{L}$).

2.5.1. Average bit error probability

From the normalized received power density function $f_{\mathcal{P}}(h)$, the statistics of the bit error probability can be obtained. Using the scalar-to-scalar conversion of variables related by monotonic functions [40], the PDF of the bit error probability can be obtained as

$$f_{\mathcal{B}}(P_e) = \left|\frac{d}{dP_e}P_e^{-1}\right| \cdot f_{\mathcal{P}}\left(P_e^{-1}\right) \tag{14}$$

where the $P_e^{-1}(P_e)$ is the inverse function of the instantaneous conditioned bit error probability. The latter can be computed for on-off keying intensity modulation direct detection (OOK IM/DD) as [41]

$$P_e(h) = \frac{1}{2}\text{erfc}\left(\frac{hP_tR}{\sqrt{2}\sigma_n}\right) \tag{15}$$

where P_t is the transmitted power, R is the responsivity of the detector, and $\sigma_n^2 = N_0R_0/R_{\text{load}}$ is the signal-independent additive white-Gaussian thermal noise (dependent on the bit rate R_0). From the PDF of the bit error probability the ABEP can be computed as

$$\text{ABEP} = \langle P_e\rangle = \int_0^{\infty} P_e(h)\, f_{\mathcal{P}}(h)\, dh = \int_0^{1/2} P_e\, f_{\mathcal{B}}(P_e)\, dP_e \tag{16}$$

where the first equality uses the channel loss PDF and the second uses the bit error probability PDF for the calculation.

2.5.2. Reliability

The reliability is defined as the probability that the instantaneous bit error probability is smaller than a certain threshold that is considered reasonable by the designer [42]. Mathematically, this parameter is computed through the PDF of the bit error probability in Eq. (14) as

$$\mathcal{L}(P_e^{\text{th}}) = \text{Prob}\left\{P_e < P_e^{\text{th}}\right\} = \int_0^{P_e^{\text{th}}} f_{\mathcal{B}}(P_e)\, dP_e \tag{17}$$

where P_e^{th} is the bit error probability threshold defined by the designer. This threshold is established depending on how the error correction code of interest performs under different levels of BEP. Usually, values on the range between $P_e^{\text{th}} \in (10^{-6}, 10^{-9})$ are considered [42].

2.5.3. Probability of outage

An outage is an event in which the data rate is above the instantaneous capacity of the channel [39]. This is equivalent to saying that there exists no error correction code that can correct the

Optics EXPRESS

instantaneous bit error probability of the channel. In this case, the channel can not handle such a data rate and the communication between the terminals fails. The outage event differs from the fade [43], in that during the outage there might be enough power to be detected by the detector, but the data can not be successfully decoded. As shown by Farid et al. [39], the probability of outage can be computed for a nonergodic slow-fading channel, OOK IM/DD modulation, and complete channel state information on the receiver as

$$P_{\text{out}}(D_0) = \text{Prob}\left[h<h_0\right] \qquad \text{with} \quad h_0 = \sqrt{\frac{C^{-1}(D_0)\sigma_n^2}{2P_t^2R^2}} \tag{18}$$

where $h = P/P_t$ is the received power normalized by the average transmitted power. D_0 is the achievable rate in bits/channel use, and represents the fraction of bits of information over all the bits sent through the channel (including the ones needed for bit error correction). The expression for the instantaneous capacity of the channel C is shown in the Supplement 1.

3. Numerical simulation of an intersatellite optical link

In this section an intersatellite free space optical link is simulated with the model presented above. First, the optimal transmitted beam is computed for minimizing/maximizing the average bit error probability, probability of outage and reliability (for each of the transmitter architectures presented in Fig. 3). Then, the performance variation under optical aberrations is studied.

3.1. Transmitted beam optimization

To have a more realistic evaluation of how the optical aberrations affect the system, the *nominal* non-aberrated transmitted beam is first computed. In this way, when computing the effect of the optical aberrations on the performance of the system, the wave physics propagation will compute the far-field irradiance due to both the truncation of the aperture and the aberrations. Previous studies have presented a Gaussian beam divergence optimization to mitigate the effects of the transmitter pointing jitter in the communication performance [7,39]. Furthermore, not only the divergence, but the shape of the far-field irradiance has also been found to be key to mitigating this effect [35]. However, these works do not consider the limitations posed by the finite sized apertures of the transmitter telescope, which are critical to determining the far-field irradiance of the beam, specially under aberrations.

The nominal non-aberrated transmitted beam is found by optimizing each performance parameter–varying the Gaussian beam shape in the transmitter aperture plane to reach the extremal value of the performance parameter. Considering the rest of the parameters to be constant, the Gaussian beam at the aperture of the transmitted telescope can be characterized by two parameters, e.g. the beamwidth w_z and the underlying beamwaist w_0 (see Fig. 3(c)). In the Supplement 1 the expression to obtain the Gaussian beam's radius of curvature R_z in the transmitter aperture plane from these two parameters is presented. Qualitatively, the beamwidth w_z is going to determine the amount of truncation that occurs to the transmitted beam while the beamwaist w_0 will determine the divergence of the untruncated pure Gaussian beam. Both together will determine the far-field irradiance field and therefore the performance of the system. In the Supplement 1 the way to adjust for these parameters, (w_0, w_z), in an equivalent optical system through ABCD matrices is presented.

For an intersatellite LEO-GEO link given by the system parameters shown in Table 1, nine optimizations are performed. Each of these optimizations corresponds to one of the three telescope architectures presented in Fig. 3 above and for each of the three performance parameters (ABEP, P_{out} and $\mathcal{L}(P_e^{\text{th}} = 10^{-6})$). Figures 5(a)-(c) show the optimization of the transmitted beam for these three performance parameters in the case of an obscured architecture (Fig. 3(a)). Furthermore, the divergence of the beam is shown in Fig. 5(d) for each point. The divergence is

Optics EXPRESS

defined as the full-width angle described by a circular contour containing the 86% of the total power of the beam as it propagates (see Supplement 1 for the formal mathematical definition). This definition is an extension of that of the pure Gaussian beam. Finally, the transmission efficiency due to the truncation of the beam on the transmitted telescope is shown in Fig. 5(e). It can be seen that the optimum for each of the parameters is given by different far-field irradiance distributions, given by different beam parameters w_z and w_0 of the transmitted beam. This is due to the fact that different far-field irradiance distributions will result in different received power statistics when combined with the pointing jitter. Each of the parameters is maximized for different received power statistics in the domain of achievable PDFs $f_{\mathcal{P}}(h)$ given by the limitations of the aperture size of the telescope and its architecture. In Fig. 5(f) the optimum far-field irradiances for each of the performance parameters are presented along with the pointing jitter PDF (due to the axially symmetrical nature of all the elements considered, the pointing jitter is also axially symmetric). In the Supplement 1, the optimization for the two remaining architectures can be found, yielding similar qualitative results. Compared to the results presented here for the obscured architecture, the clear aperture case yields better values of the performance parameters, primarily due to the higher power available after the truncation and obscuration of the beam. In the subaperture case, the interplay between the achievable divergence and the power loss due to the truncation, also limits the performance of the system compared to the clear aperture case.

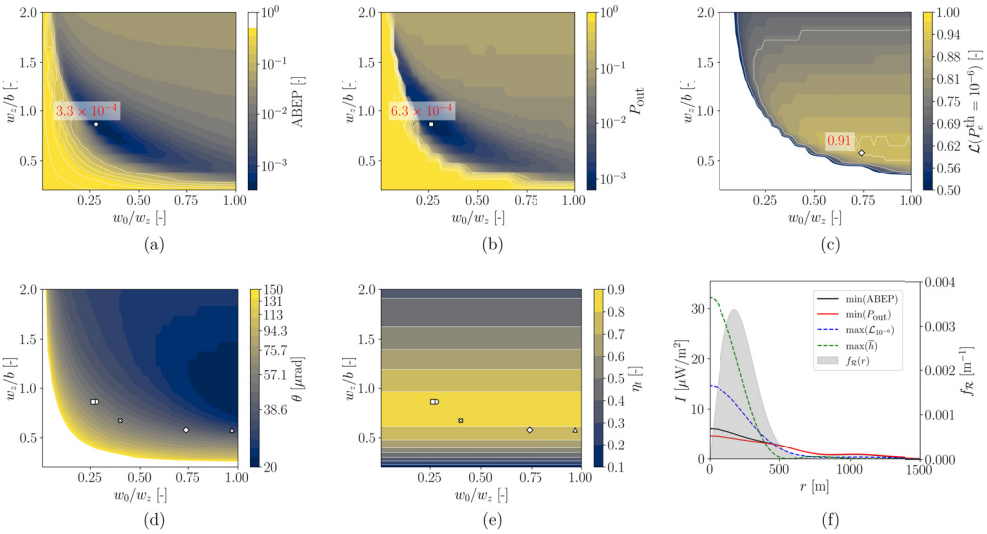

Fig. 5. Optimization of the transmitted beam for an intersatellite link given by the parameters in Table 1 and the telescope architecture shown in Fig. 3(a). (a), (b), and (c) are the optimizations for each of the performance parameters considered. (d) and (e) show the transmitted beam divergence and the telescope transmission efficiency due to the truncation, respectively. The cross and the triangle give the optimum for $\mathcal{L}(P_e^{\text{th}} = 10^{-3})$ and $\mathcal{L}(P_e^{\text{th}} = 10^{-9})$ respectively. (f) are the far field irradiances as a function of the radial coordinate in the receiver aperture plane for the optimum points found in (a)-(c), along with the irradiance field that maximizes the received power average $\overline{h}$, and the PDF $f_{\mathcal{R}}(r)$ of the pointing jitter.

From the analysis above it can be seen that the optimum characteristics of the Gaussian beam in the transmitter aperture plane, are extremely dependent on the performance parameter that is being optimized. For minimization of the ABEP and the probability of outage, it can be seen that more uniform distributions of the far-field are interesting. This is due to the underlying received power

Optics EXPRESS

Table 1. Parameters used for an intersatellite LEO-GEO free space optical link.

Parameter	Value	Ref.	Parameter	Value	Ref.
λ	1550 nm	-	b	6.75 cm	[44]
P_t	10 W	-	a	$\{0, 1.35\}$ cm	-
σ_n	4.7×10^{-9} V	[35]	Modulation	OOK-NRZ	[35]
σ_θ	5 μrad	[45]	Data rate	10 Gbps	[35]
R	0.8153 A/W	[33]	Δz	36000 km	-

statistics given by these type of far-field irradiances. For a spatially more uniform (compared to Gaussian) type of far-field irradiance distributions, the resulting receive power statistics are more condensed around a central received power. In the limit of perfectly uniform far-field irradiance, the received power statistics would be given by a discrete probability distribution. In the case of outage probability, this tendency is justified by the fact that the Eq. (18) sets a minimum received power threshold above which any extra power is not beneficial for this performance parameter. In the case of the ABEP, the results show that there is a trade-off between the maximum achievable received power and the uniformity of the beam. This is in agreement with the findings in [35]. Furthermore, the divergence value of 52.8 μrad obtained for the minimum ABEP (circled marker in Fig. 5(d)), is in close agreement with the 51.6 μrad that would be obtained using Eq. (12) in [7]. The discrepancy between these two values is due to the non-Gaussian beam shape resulting from the truncation of the beam considered in the present paper.

For maximizing the reliability, the figure shows that a more Gaussian shape is beneficial. This means that the underlying received power statistics for maximizing this parameter are much more skewed than in the cases before. This effect is more pronounced as the bit error probability threshold of the considered reliability decreases (see Supplement 1). However, attending to Eqs. (18) and (17) it can be seen that the reliability and the probability of outage are mathematically similar, in that they set a power threshold above which the performance of the system is considered acceptable. Then, the probability of being above (or below) this power threshold is maximized (or minimized). Hence, given the similar mathematical expression for the computation of these two parameters, we would expect a similar type of far-field irradiances in contrast to what is shown in Fig. 5(f). The discrepancy between the far-field irradiances for outage probability and reliability is due to the different power thresholds set by each of these parameters. While reliability is a much more practical parameter, it establishes a receive power threshold way above the one set by the probability of outage. The later being a theoretical limit in which failure would occur due to information theoretical restrictions. Due to the power threshold of the reliability being higher to that of the probability of outage, the physical limits imposed on the Gaussian beam source are not able to uniformize the beam for the reliability power threshold as it did for the probability of outage. Hence, the physical limitations imposed (truncated Gaussian beam in the transmitter aperture plane) yield a more Gaussian beam shape far-field irradiance for the reliability threshold compared to the optimum beamshape for the probability of outage. This is in agreement with the tendency shown for the $P_e^{\text{th}} = 10^{-3}$ and $P_e^{\text{th}} = 10^{-9}$ shown in the Supplement 1, showing that the reliabilities and the probability of outage belong to the same family of parameters (the one that set a power threshold and computes the cumulative density function of it).

To emphasize the improvement provided by the optimization proposed, a comparison with a baseline truncated Gaussian beam is now discussed. The baseline beam considered is the one that maximizes the average received power $\overline{h}$. The maximization of $\overline{h}$ is in line with the maximization of the peak of the irradiance field at the receiver aperture plane, which is the parameter considered in previous works [10,46]. The far field irradiance of the baseline result can be seen in Fig. 5(f),

Optics EXPRESS

for the obscured architecture. In the Supplement 1 the far-field irradiances and received power PDF of all the architectures can be found. Table 2 summarizes the improvement on each of the parameters that the proposed optimization can provide for different architectures, in comparison to the baseline field obtained by maximizing the received power average $\bar{h}$. It can be seen that the optimized fields result in perform various orders of magnitude better in terms of ABEP and P_{out}. Furthermore, it is also seen that a bigger relative improvement is provided by the optimization in the clear and subaperture architectures, compared to the obscured architecture. In summary, these results highlight the relevance of optimizing the optical system attending to communication performance parameters, instead of attending widely used optical imaging performance parameters (e.g. peak irradiance, Strehl ratio).

Table 2. Improvement provided by the optimization compared to the baseline field performance, given by the field that maximizes the average received power $\bar{h}$.

	Obscured	Clear	Subaperture
$\text{ABEP}_{\max(\bar{h})}/\min(\text{ABEP})$	46.5	5.7×10^2	4.3×10^2
$P_{\text{out},\max(\bar{h})}/\min(P_{\text{out}})$	77.2	9.8×10^4	1.7×10^4
$\max(\mathcal{L}_{10^{-6}})/\mathcal{L}_{10^{-6},\max(\bar{h})}$	1.03	1.06	1.11

3.2. Seidel optical aberrations

To assess the effect of optical aberrations on intersatellite links, that will enable setting requirements for admissible optical aberrations on intersatellite terminals, the optimum outgoing beams computed in the previous section are perturbed with Seidel aberrations. Using now the full model presented in Fig. 2, the effect of these aberrations are computed independently of each other yielding the results shown in Fig. 6. Firstly, several qualitative differences can be discerned between the subaperture architecture (third row) and the rest. In the case of the former, as the symmetry of the transmitted beam is broken with respect to the telescope's optical axis, the coma aberrations that are defined over the whole aperture of the telescope do not have the same effect. That symmetry breaking, due to the non-axially symmetric transmit field, creates unequal behaviors of the horizontal and vertical commas as seen in Fig. 6(g)-(i).

In general, for all the architectures, coma aberration seems to be the one that has the highest impact on the performance of the system. This effect is expected as coma is the only Seidel aberration creating an apparent angle of arrival. Hence, coma aberration is the only one creating a systematic boresight pointing error of the transmitted beam. The fields in the transmitter aperture plane, far-field receiver plane and the tracking sensor plane for the case of vertical coma aberration are shown in Fig. 7. In this figure we can see more clearly the differences between the clear and subaperture architectures (Figs. 7(b) and (c), respectively). The Gaussian beam in the clear aperture architecture is truncated symmetrically around its axis, while in the subaperture case the truncation occurs in a non-symmetric way. We have considered the same diameter for the aperture in both architectures, and hence the effective diameter achievable without clipping is smaller for the subaperture architecture. This is why in the subaperture architecture the limitation of an smaller effective diameter is mitigated by choosing a more collimated beam in the transmitter's aperture for the nominal case (compare the optimum ratios w_0/w_z in Fig. S7 and S8 on the Supplement 1). Furthermore, while the apparent angle of arrival is the same in both cases for the same optical aberration, the transmitted beam on the subaperture architecture is only affected by a local section of the full optical aberration.

Furthermore, the effect of defocus aberration is analogous to changing the radius of curvature of the transmitted beam, and this in turn is equivalent to changing the beamwaist w_0 of the transmitted beam. As these parameters have been optimized as shown in the previous section,

Optics EXPRESS

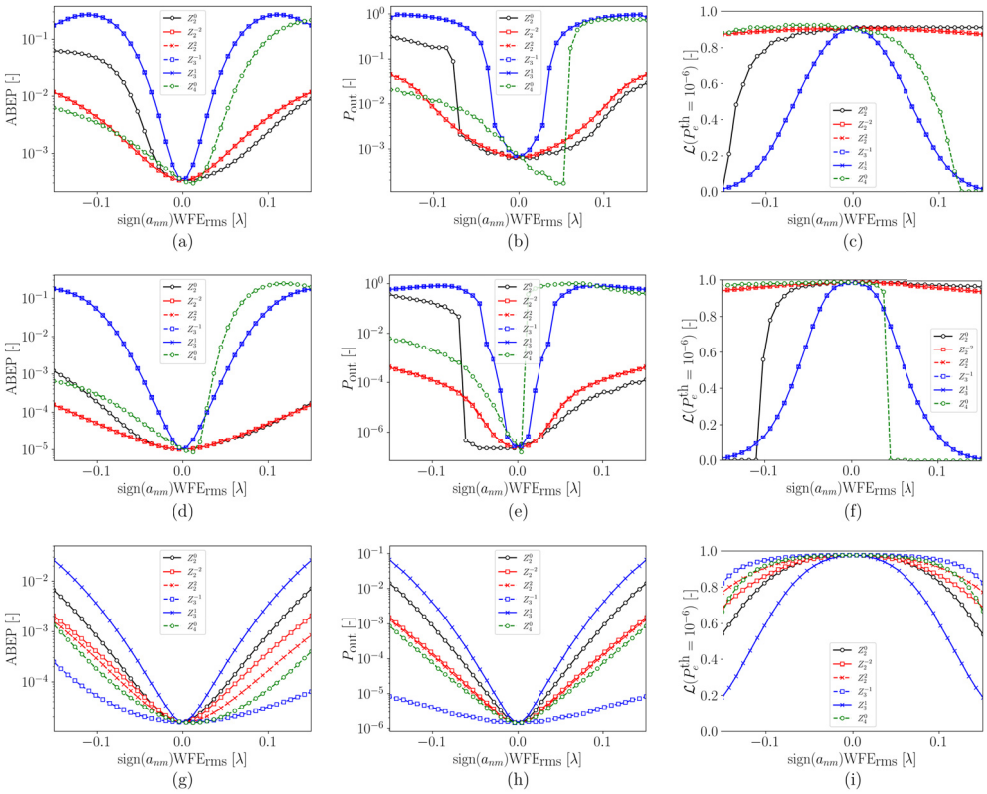

Fig. 6. Effect of optical aberrations on the performance of a LEO-GEO intersatellite link. First, second and third rows correspond to the obscured, clear, and subaperture architectures respectively.

defocus has the same effect as traveling in w_z constant lines in Fig. 5(a)-(c). As the outgoing beam is optimized before any aberrations are applied, the effect of further defocus is to detriment the respective performance parameter as shown in Fig. 6. Finally, it is relevant to mention that the effect of a slight spherical aberration can be beneficial in some cases as is shown for all the parameters in the obscured and clear aperture cases (rows one and two in Fig. 6). This is in agreement with the findings reported in Ref. [35] in which a redistribution of the far-field irradiance, reducing the peak irradiance and transferring it towards the outside of the beam, can be beneficial for mitigating the pointing jitter. This is indeed the effect of spherical aberration [38].

Although the results presented for each of the aberrations applied independently provide insight into the physics behind this perturbation, in reality, the optical aberrations that will appear on telescopes due to thermo-mechanical loads are a combination of all these aberrations [10]. In order to evaluate statistically the admissible values for the root mean square of the optical aberrations, Monte Carlo simulations for combinations of all the Seidel aberrations have been considered in a similar manner as done by Kenny et al. for the LISA gravitational interferometry mission [47]. The results of these Monte Carlo simulations are shown in Fig. 8. This simulations are performed by randomly allocating to each aberration a wavefront error root mean square magnitude coming from a uniform distribution, in accordance to the experimental results presented in [10]. It can be seen that the less sensitive architecture of all is the subaperture architecture in which both the percentiles and the mean remain the most unaffected by the increasing magnitude of the optical

Optics EXPRESS

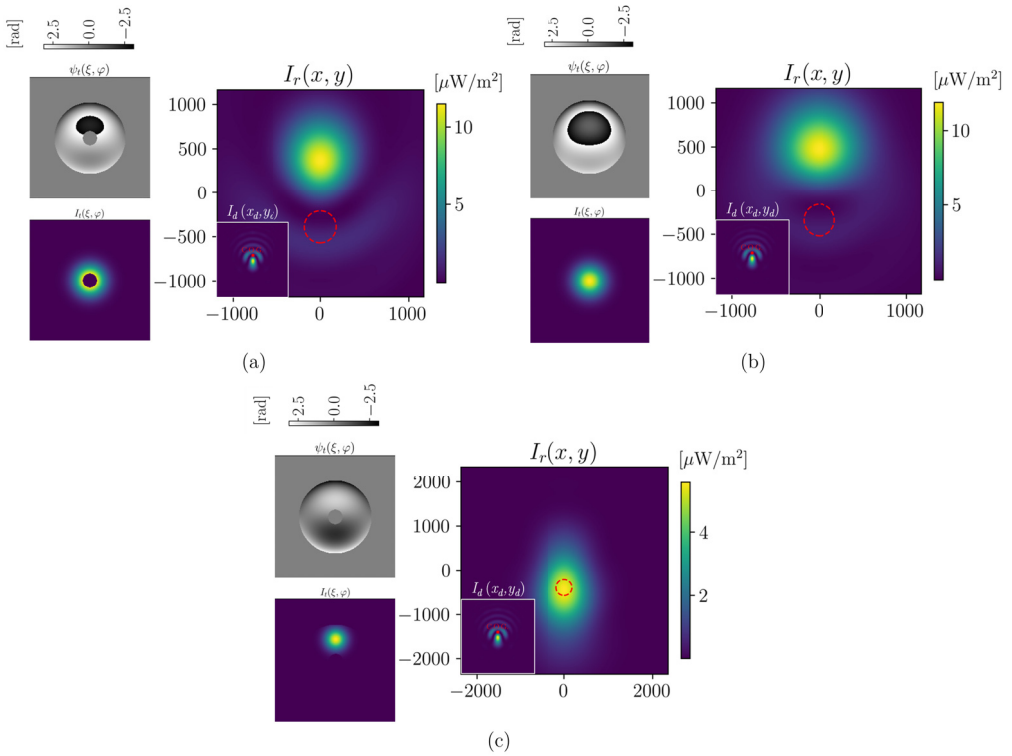

Fig. 7. Fields in the case of vertical coma aberration with $\mathrm{WFE}_{\mathrm{rms}} = 0.15\ \lambda$ for (a) obscured, (b) clear and (c) subaperture architectures respectively. The small figures on the left show the transmitter aperture phase and irradiance. The big figure shows the far-field irradiance in the receiver aperture planes along with a red circle enclosing the area of $<1\sigma$ of the pointing jitter (the center of which is the computed static boresight error due to the apparent angle of arrival). The receiver is located at the origin in the receiver aperture plane. The snippet shows the tracking sensor irradiance field.

aberrations. This is due to the fact that the Zernike polynomials are defined over the whole aperture of the transmitter telescope, while the transmitted beam in the subaperture architecture only uses a small section of this aperture. Hence, the Seidel aberrations on the whole aperture basis are seen as similar to a combination of tip-tilt and astigmatism in the transmitted Gaussian beam basis. The results presented enable us to discern the effect of optical aberrations in the apparent angle of arrival and the far-field irradiance. Using the reliability $\mathcal{L}$ for the sake of the explanation, the apparent angle of arrival is the same in both the obscured and subaperture architectures. However, the effect of the optical aberrations is much more pronounced in the obscured case as seen in Fig. 8(c). This means that the alterations of the far-field irradiance generated by the optical aberrations have a determining role in the performance of the system. This effect can also be seen by comparing the clear and subaperture architectures in the same figure. We can see in Figure S4 of the Supplement 1, that the difference on the apparent angle of arrival for the clear and subaperture cases is very similar. Therefore, the much higher sensitivity of the clear aperture architecture to the performance parameters shown in Fig. 8 can only be due to the effect of the Seidel aberrations on the transmitted beam. As for the obscured case, the transmitted beam in the clear aperture case is also subjected to full aberrations (see Fig. 6(a)-(b)). In contrast, the transmitted beam on the subaperture architecture is only affected by a localized

Optics EXPRESS

section of the full aberrations (see Fig. 6(c)). By using simulations as the ones shown in Fig. 8, the requirements for acceptable wavefront errors can be determined for optical terminals working as transmitters. However, when the terminal is also working as a receiver the effects of optical aberrations in the received beam when coupling it to the detector also need to be considered.

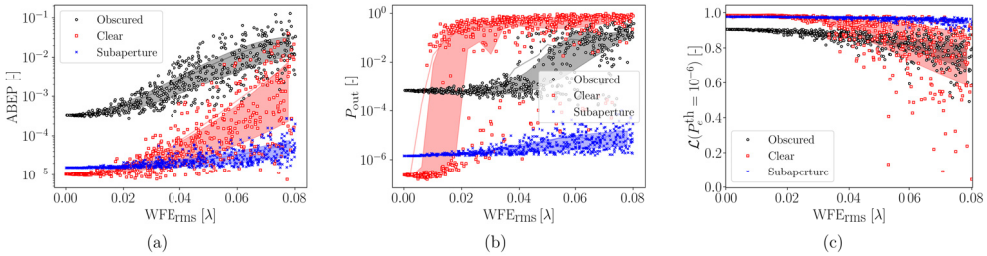

Fig. 8. Effect of optical aberrations in the performance of a LEO-GEO intersatellite link given by Monte Carlo simulations of the Seidel aberrations. The circle markers show the Monte Carlo simulations, while the mean is given by a solid fitted curve and the 25% and 75% percentiles are bounding the filled areas.

For the sake of better understanding how the results presented in Fig. 8 can be used, an evaluation of the performance of the system is done when under Maréchal's criteria. Maréchal's criteria is determined by assuring that the peak irradiance of the diffraction pattern of a uniform circular aperture under aberrations is reduced by less than 20%. This in turn yields a maximum allowable aberration given by $\text{WFE}_{\text{rms}} \leq \lambda/14$ [48]. This criteria is in principle only useful for imaging optical systems, as it does not account for truncated Gaussian beams, stochastic pointing jitter and captured power statistics. However, we can now evaluate the adequacy of Maréchal's criteria to an intersatellite optical communication system. By considering the effect that optical aberrations have on the reliability shown in Fig. 7, we can see that average of the reliability in the clear architecture goes from 98.4% in the non aberrated case, to 72.4% in the limiting Maréchal condition. The latter architecture is the one that is most affected as the obscured and subaperture architectures go from 90.4% and 97.3% to 77.8% and 95.3%, respectively. By extending this analysis to the performance parameter of interest we can understand what imposing the classical diffraction-limited condition (Maréchal's condition) used in imaging optics, means on the design of optical communication terminals. All things considered, in order to evaluate the effect of optical aberrations on intersatellite optical links, it is paramount to use a complete end-to-end model that considers altogether this coupled phenomena.

4. Conclusions and further work

We have presented in this work a complete framework that models the coupled effects of the transmitter pointing jitter and optical aberrations on intersatellite free space optical communications. The model presented enables the evaluation of the effect of these perturbations in the communication performance of the system, i.e. average bit error probability, probability of outage and reliability. Three different architectures have been analyzed, namely the obscured, clear, and subaperture architectures. Firstly, an optimization of the transmitted Gaussian beam considering the transmitter pointing jitter and the finite aperture effects (without optical aberrations) has been performed. This optimization shows that the optimum far-field irradiances depend on the communication parameter chosen as the target. Indeed, non-Gaussian beams generated by using the aperture truncation effects of the transmitter telescope are beneficial in some of these optimizations. Finally, the full framework developed has been used to evaluate the effect of the optical aberrations, by perturbing the previously obtained optimal beams with different Seidel aberrations. It has been found, that the effect of coma is extremely detrimental as a result of the

Optics EXPRESS

apparent angle of arrival created. Finally, given that in practical scenarios these aberrations will appear altogether, Monte Carlo simulations of combinations of Seidel aberrations are presented to statistically determine the impact of optical aberrations in the system performance. The latter will help to determine the requirements of admissible optical aberrations on intersatellite free space optical communication terminals. Among the challenges encountered in this work, the authors would like to highlight the large computational cost required for the simulations presented, that required the use of a supercomputer [49]. Moreover, the convergence of the numerical code requires a proper tuning of the numerical parameters (e.g. grid size for the Fresnel propagation or bin size of the computed PDFs) that is dependent on the parameters of the link (Table 1).

It is the authors' recommendation to further research the coupled effects of optical aberrations and receiver angle of arrival on the receiving terminal and expand the results obtained here to other applications and use cases such as space-to-earth downlink (considering atmospheric effects and other modulation schemes) and quantum communications.

Funding. Nederlandse Organisatie voor Wetenschappelijk Onderzoek (P19-13).

Acknowledgment. M.B. would like to thank Juan Reto Reynal for the useful discussions during the process of writing this paper. The authors acknowledge the use of computational resources of the DelftBlue supercomputer, provided by Delft High Performance Computing Centre.

Disclosures. The authors declare no conflicts of interest.

Data availability. Data underlying the results presented in this paper are not publicly available at this time but may be obtained from the authors upon reasonable request.

Supplemental document. See Supplement 1 for supporting content.

References

1. S. Khatri, A. J. Brady, R. A. Desporte, *et al.*, "Spooky action at a global distance: analysis of space-based entanglement distribution for the quantum internet," npj Quantum Inf. **7**(1), 4–15 (2021).
2. H. Du, K. Cao, J. Ding, *et al.*, "A new statistical fading model for loss factor induced by angle-of-arrival fluctuations in free space optical communication," Opt. Express **32**(14), 24926–24946 (2024).
3. Y. Yang, L. Tan, J. Ma, *et al.*, "Effects of localized deformation induced by reflector antenna on received power," Opt. Commun. **282**(3), 396–400 (2009).
4. W. Xie, L. Tan, J. Ma, *et al.*, "Received power analysis due to antenna deformation based on wavelet in inter-satellite laser communication links," Optik **123**(8), 670–674 (2012).
5. Y. Yang, G. Cao, and H. Zhao, "Influence of localized distortion in lenses on Strehl ratio in lasercom," Optik **124**(23), 6415–6418 (2013).
6. K. Kiasaleh, "On the probability density function of signal intensity in free-space optical communications systems impaired by pointing jitter and turbulence," Opt. Eng. **33**(11), 3748–3757 (1994).
7. M. Toyoshima, T. Jono, K. Nakagawa, *et al.*, "Optimum divergence angle of a Gaussian beam wave in the presence of random jitter in free-space laser communication systems," J. Opt. Soc. Am. A **19**(3), 567–571 (2002).
8. Y. Zhu, G. Xu, M. Gao, *et al.*, "Average bit-error rate analysis of an inter-satellite optical communication system under the effect of perturbations," Opt. Express **32**(21), 36796–36810 (2024).
9. G. Xu, L. Yin, Y. Zhu, *et al.*, "Satellite-to-ground optical communication systems under orbital deviations and atmospheric turbulence: channel modeling and performance analysis," Opt. Express **33**(9), 18912–18927 (2025).
10. M. Toyoshima, N. Takahashi, T. Jono, *et al.*, "Mutual alignment errors due to the variation of wave-front aberrations in a free-space laser communication link," Opt. Express **9**(11), 592–602 (2001).
11. J. Sun, L. Liu, M. Yun, *et al.*, "Mutual alignment errors due to wave-front aberrations in intersatellite laser communications," Appl. Opt. **44**(23), 4953–4958 (2005).
12. Y. Yang, L. Tan, and J. Ma, "Mutual alignment errors due to localized distortion in free-space laser communication links," Opt. Commun. **281**(17), 4180–4187 (2008).
13. L. Tan, Y. Yang, J. Ma, *et al.*, "Pointing and tracking errors due to localized deformation in inter-satellite laser communication links," Opt. Express **16**(17), 13372–13380 (2008).
14. Y. Yang, L. Tan, and J. Ma, "Pointing and tracking errors due to localized distortion induced by a transmission-type antenna in intersatellite laser communications," Appl. Opt. **48**(4), 786–791 (2009).
15. A. Yoshida, "Spherical aberration in beam optical systems," Appl. Opt. **21**(10), 1812–1816 (1982).
16. V. N. Mahajan, "Uniform versus Gaussian beams: a comparison of the effects of diffraction, obscuration, and aberrations," J. Opt. Soc. Am. A **3**(4), 470–485 (1986).
17. P. J. Cronin, P. Török, P. Varga, *et al.*, "High-aperture diffraction of a scalar, off-axis Gaussian beam," J. Opt. Soc. Am. A **17**(9), 1556–1564 (2000).

Optics EXPRESS

18. E. Cojocaru, V. Draganescu, and N. Herisanu, "Astigmatism together with longitudinal focal shift in off-axis optical systems," Appl. Opt. **29**(28), 4208–4211 (1990).
19. S. C. Biswas and J.-E. Villeneuve, "Diffraction of a laser beam by a circular aperture under the combined effect of three primary aberrations," Appl. Opt. **25**(13), 2221–2232 (1986).
20. Y. Yang, Q. Han, L. Tan, *et al.*, "Influence of wave-front aberrations on bit error rate in inter-satellite laser communications," Opt. Commun. **284**(12), 3065–3069 (2011).
21. Y. Yang, Q. Han, L. Tan, *et al.*, "Research on bit error rate in the presence of local wavefront aberration in intersatellite laser communications," J. Lightwave Technol. **29**(19), 2893–2898 (2011).
22. A. Alvarez-Herrero, T. Belenguer, L. Pascual, *et al.*, "Conceptual optical design for CARAMUEL payload: a quantum key distribution system from a GEO satellite," Proc. SPIE **12633**, 126330B (2023).
23. K. Niu and C. Tian, "Zernike polynomials and their applications," J. Opt. **24**(12), 123001 (2022).
24. J. W. Goodman, *Introduction to Fourier optics* (Roberts & Co., 2005).
25. H. Rabal, N. Bolognini, and E. Sicre, "Diffraction by a tilted aperture," Opt. Acta: Int. J. Opt. **32**(11), 1309–1311 (1985).
26. K. Patorski, "Fraunhofer diffraction patterns of titled planar objects," Opt. Acta: Int. J. Opt. **30**(5), 673–679 (1983).
27. K. Matsushima, H. Schimmel, and F. Wyrowski, "Fast calculation method for optical diffraction on tilted planes by use of the angular spectrum of plane waves," J. Opt. Soc. Am. A **20**(9), 1755–1762 (2003).
28. Y. Hu, X. Liu, X. Liu, *et al.*, "Diffraction modeling between arbitrary non-parallel planes using angular spectrum rearrangement," Optica **12**(1), 39–45 (2025).
29. M. Badás, P. Piron, J. Bouwmeester, *et al.*, "Opto-thermo-mechanical phenomena in satellite free-space optical communications: survey and challenges," Opt. Eng. **63**, 041206 (2023).
30. X. Wang, X. Wang, C. Li, *et al.*, "Angular micro-vibration of the Micius satellite measured by an optical sensor and the method for its suppression," Appl. Opt. **60**(7), 1881–1887 (2021).
31. K. Riesing, C. M. Schieler, J. Brown, *et al.*, "Pointing, acquisition, and tracking for the TBIRD CubeSat mission: system design and pre-flight results," in *Proc. SPIE*, vol. 11993 (San Francisco, United States, 2022), pp. 1–10.
32. P. F. I. Scott, A. S. Kachatkou, N. R. C. Kyele, *et al.*, "Real-time photon beam localization methods using high-resolution imagers and parallel processing using a reconfigurable system," Opt. Eng. **48**(7), 073601 (2009).
33. T. Song, Q. Wang, M.-W. Wu, *et al.*, "Impact of pointing errors on the error performance of intersatellite laser communications," J. Lightwave Technol. **35**(14), 3082–3091 (2017).
34. I. U. Zaman and O. Boyraz, "Impact of receiver architecture on small satellite optical link in the presence of pointing jitter," Appl. Opt. **59**(32), 10177–10184 (2020).
35. M. Badás, P. Piron, J. Bouwmeester, *et al.*, "On the optimum far-field irradiance distribution using Laguerre-Gaussian beams for intersatellite free-space optical communications," Opt. Express **32**(18), 31597–31620 (2024).
36. R. D. Nelson, T. H. Ebben, and R. G. Marshalek, "Experimental verification of the pointing error distribution of an optical intersatellite link," in *Proc. SPIE*, vol. 885 (1988), pp. 132–142.
37. M. Toyoshima, Y. Takayama, H. Kunimori, *et al.*, "In-orbit measurements of spacecraft microvibrations for satellite laser communication links," Opt. Eng. **49**(8), 083604 (2010).
38. M. Badás, J. Bouwmeester, P. Piron, *et al.*, "Impact of transmitter wavefront errors and pointing jitter on intersatellite free space optical communications," Proc. SPIE **13023**, 1302302 (2024).
39. A. A. Farid and S. Hranilovic, "Outage capacity optimization for free-space optical links with pointing errors," J. Lightwave Technol. **25**(7), 1702–1710 (2007).
40. J. B. Thomas, *Introduction to Probability* (Springer, 1986).
41. S. B. Alexander, *Optical communication receiver design* (SPIE, 1997).
42. A. A. Farid and S. Hranilovic, "Link reliability, range and rate optimization for free-space optical channels," in *2009 10th International Conference on Telecommunications*, (2009), pp. 19–23.
43. R. R. Hayes, "Fading statistics for intersatellite optical communication," Appl. Opt. **36**(30), 8063–8068 (1997).
44. F. Heine, A. Brzoska, M. Gregory, *et al.*, "Status on laser communication activities at Tesat-Spacecom," Proc. SPIE **12413**, 124130C (2023).
45. K. Cahoy, P. Grenfell, A. Crews, *et al.*, "The CubeSat Laser Infrared CrosslinK Mission (CLICK)," Proc. SPIE **11180**, 111800Y (2019).
46. H. T. Yura, "Optimum truncation of a Gaussian beam in the presence of random jitter," J. Opt. Soc. Am. A **12**(2), 375–379 (1995).
47. F. Kenny and N. Devaney, "Beam propagation simulations for LISA in the presence of telescope aberrations," Classical Quantum Gravity **38**(3), 035010 (2021).
48. E. Wolf, "The diffraction theory of aberrations," Rep. Prog. Phys. **14**(1), 95–120 (1951).
49. Delft High Performance Computing Centre (DHPC), "DelftBlue Supercomputer (Phase 2)," https://www.tudelft.nl/dhpc/ark:/44463/DelftBluePhase2 (2024).